LUND UNIVERSITY
Faculty of Science

Improving image quality of a streak camera using periodic shadowing

David Lange

Thesis submitted for the degree of Bachelor of Science
Project duration: 4 months

Supervised by Andreas Ehn and Joakim Bood

Department of Physics
Division of Combustion Physics
February 2020

Abstract

Stray light suppression using a method inspired by lock-in amplification, called periodic shadowing, is examined and demonstrated for a measurement involving a streak camera. The experiment consists of resolving the fluorescent decay of the dye Rhodamine B (RhB) and examining both the rise and the decay of the fluorescence. A simple mono exponential model is fitted to determine the lifetime of the decay in the temperature range 20°C - 74°C. These novel results show that periodic shadowing is easy to implement in streak camera measurements and it significantly improves measurement data.

Acronyms

CCD Charge-coupled device.

LIF Laser induced fluorescence.

MCP Microchannel plate.

MCP-PMT Microchannel plate photomultiplier tube.

PMT Photomultiplier tube.

RhB Rhodamine B.

Contents

1 Introduction

Since the invention of the laser in the 1960s, the laser has quickly established itself as a powerful tool in research and also has led to the development of a variety of technical applications in industry nowadays. Figure 1 shows the basic schematic of common lasers such as the Nd:YAG-Laser.

One important application of lasers is spectroscopy. Atoms and molecules have unique quantum states that can be stimulated by photons of specific wavelength. In spectroscopic measurements, certain atoms or molecules are targeted by tuning the laser to a wavelength corresponding to a quantum state of interest.

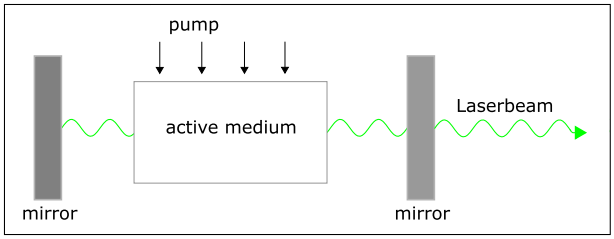

Figure 1: Basic laser scheme: An active medium is pumped, e.g. by a flash lamp. The mirrors are placed to fulfill the standing wave condition, one of the mirrors is not fully reflective so part of the wave can escape. Since the mirrors are planar, the exiting laserbeam is highly collimated. The active medium can be chosen, so that a specific radiative transition is targeted. The result is the main feature of the laser: That the photons in the cavity have the same wavelength and are in phase.

Applications range to many areas of applied physics, such as calibration of telescopes and to industrial applications like material processing [1]. Because of the laser's ability to be tuned very precisely to specific wavelengths, it is especially powerful in lifetime measurements of specific transitions in atoms or molecules. Measurement techniques based on fluorescence lifetime imaging could be of interest in, for example, microfluidics, where temperature and pressure fields can be utilized for flow control.

Microfluidics is the study of fluids constrained into small space, known as microchannels, where effects neglected in classical fluid dynamics become relevant. Such phenomena arise due to that surface properties become more significant, since surface and bulk are now at similar scales. Microfluidics enable biologists to study and classify substances on cellular level, by driving a microchannel, e.g. with ultrasound [2]. This technique can be used, for example, to separate cells placed in a microchannel, since different substances have distinct acoustic impedances and thus disturb the induced acoustic field in different ways [3]. Research is also being conducted on understanding the effects that pressure or temperature fields have on microchannels. One approach to induce temperature gradients in liquids can be achieved by mixing a fluorescent tracer substance into the microfluid and then use a laser to excite the tracer. Most of the energy that is induced by the laser will be transferred to heat through collisional quenching. A second tracer that has a temperature sensitive fluorescence lifetime, can then be added to the liquid and works as a thermometer by relating the fluorescent lifetime to the temperature [4].

Photon detection devices such as photodiodes, PMTs and MCP-PMTs are able to make temporally resolved point measurements whereas intensified CCD cameras can be used for two dimensional measurements [5]. A rather unique detector, which offers both temporal and spatial resolution, is the streak camera. Today, the temporal resolution of a streak camera reaches a few hundred femtoseconds [6]. As with all detectors, the streak camera suffers from

limitations in resolution and contrast. The sophisticated design of the streak camera, with several processing steps in between photon detection and spatiotemporal resolved data generation, results in reduction in contrast, which affects both temporal and spatial resolution. Such imperfections originate from unwanted signal scattering inside the streak camera, that makes the path of some of the signal photons deviate and disturb the final measurement data. One method that has been used to significantly reduce stray light in spectrometers is periodic shadowing, by using a signal coding/decoding processing scheme [7]. The signal is modulated analogically before entering the spectrometer and later demodulated as part of a post processing step. Analogically here means, that a grating is mounted onto the slit, through which the light is entering the spectrometer.
This thesis involves two tasks: (1) investigating if the contrast of the streak camera can be improved by using periodic shadowing by (2) investigating the temperature sensitivity of Rhodamine B in water.

2 Background

The laser system consists of a Nd:YAG picosecond pulsing laser. The streak camera used in this investigation, as well as a method to achieve high amplitude laser pulsing, called mode-locking is described in this section. Furthermore, the fluorescence dye used, Rhodamine B, will be briefly characterized and correspondingly Laser induced fluorescence explained.

2.1 Mode-locking

Mode-locking is a technique to achieve laser pulses with high intensity and short temporal duration, on the order of pico- to femtoseconds. The technique is based on coupling of different oscillating modes in the laser cavity by matching their phase. A qualitative picture of some oscillations is shown in figure 2. Without mode-locking, the different modes would interfere constructively and destructively in the optical resonator, resulting in a random amplitude distribution of the electric field. [8]

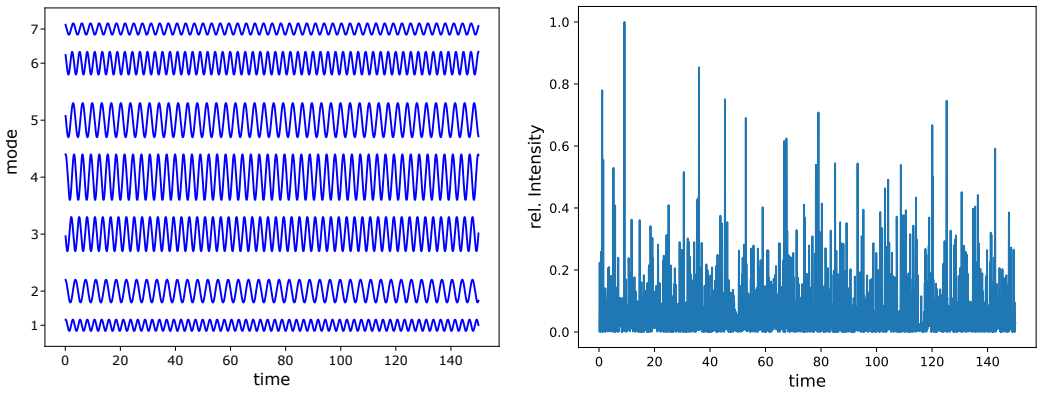

Figure 2: a.) Qualitative picture of a number of oscillations. b.) Sum of a larger number of random oscillations (N = 100). Reproduced from [8].

However, to achieve a maximum amplitude output, it is desired to have constructive interference of all the different mode's anti-nodes at times. This can be achieved by locking the phases of all modes relative to each other. Such a scheme gives a resulting pulse train of very high electric field amplitudes.
Mathematically, the different modes can be viewed as components of a Fourier series, and the variation of intensity in time of the resulting superposition is given by [9]

$$I(t) = \left| \sum_{m=0}^{m=M} A_m \cdot \exp\left(i\left(\omega_m \cdot t + \phi_m\right)\right) \right|^2, \tag{1}$$

where m is the mode number, A_m it's amplitude, ω the corresponding frequency and ϕ_m the corresponding phase. In the Fabri-Perot resonator, the spacing of the different longitudinal modes is given by

$$\delta f = c/2nL, \tag{2}$$

where c is the speed of light in vacuum, n the refractive index of the medium and L the distance between the mirrors. A modulator couples the phases to each other and equation 1 becomes

$$I(t) = \left| \sum_{m=-N}^{m=N} A_m \cdot \exp\left(i\left(\left(\omega_0 + m \cdot \delta f\right) \cdot t + \phi\right)\right) \right|^2, \tag{3}$$

with ω_0 being the central frequency of the light wave and ϕ the coupled phase difference. The technical term for this type of coupling is active mode-locking. The modulator, mentioned above, acts like a trigger for the cavity by synchronizing its modulation frequency to the roundtrip in the cavity. By doing so, cavity conditions are only satisfied for a very short period of time during each roundtrip and thus only one bunch of photons are able to grow in numbers to form a short laser pulse.
Under certain conditions, equation (3) can describe a pulse train. One of these conditions is, to set $\phi = 0$ and A_m to a constant A for all modes. The resulting intensity can be written as

$$I(t) = A^2 \frac{\sin^2\left(\delta f \cdot t(N + 1/2)\right)}{\sin^2\left(\delta f \cdot t/2\right)}. \tag{4}$$

Figure 3 shows a pulse train construction using equation (4).

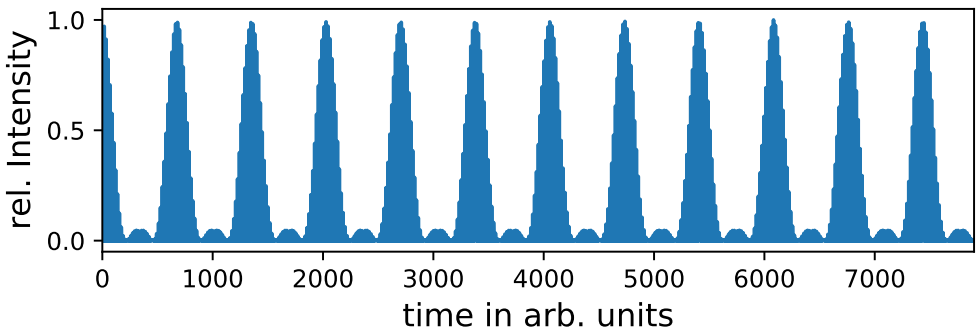

Figure 3: Pulse train construction using the derived equation (4) with $N = 1000$ and $L = 0.05$ m in eq. (2).

2.2 Streak camera

Figure 4 shows the main parts of a streak camera and should be viewed from left to right. Photons pass through an adjustable slit and are directed and focused onto a photocathode where they are converted into photo-electrons. Immediately thereafter, the photo-electrons enter the MCP, a micro-channel plate, which is used to multiply the number of electrons by generating secondary electrons.
These electrons get further accelerated until they pass a pair of deflecting electrodes. High voltage is ramped up as the photo-electrons pass between the electrodes. The sweep voltage is well defined in time and synchronized with the incident light. The photoelectrons that arrive early, are deflected less than the electrons that arrive later. Thus, a time dimension can be extracted from the measurement. Next, these electrons hit a phosphor screen which induces a photon base signal that is guided to a CCD chip where the signal is stored. The image created on the phosphor screen is called the streak image. The time difference of the successive incident photons can be reconstructed as well as a one dimensional relative position, as shown in figure 4. It is worth mentioning that the entrance slit is a double edged sword: The slit width determines how much light can enter, thus is responsible for the signal-to-noise ratio. However, if the chosen slit is too wide, the voltage sweep loses accuracy and the temporal resolution is compromised.

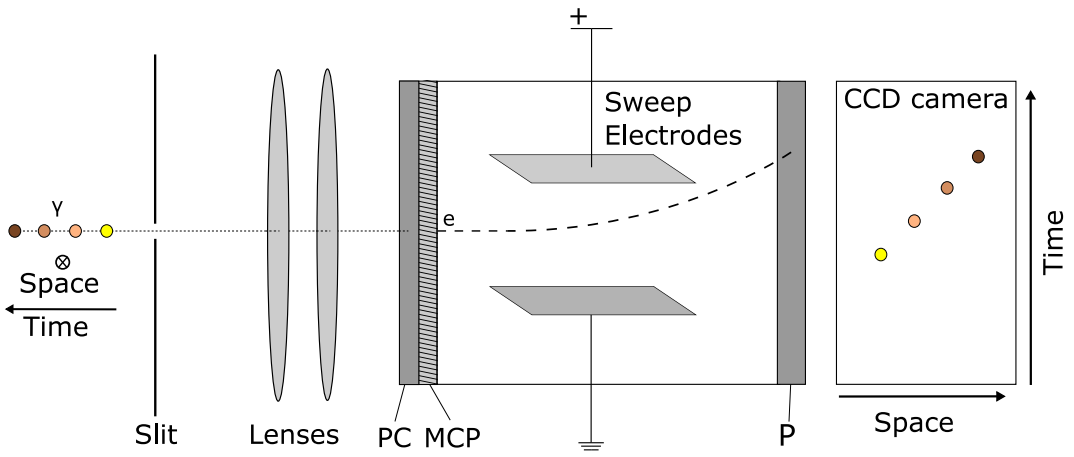

Figure 4: Scheme of the used streak camera. PC is the photo-cathode and P the phosphor-plate. Reproduced from [5], [6].

The streak camera can also be used to perform time-resolved spectroscopy, by coupling the entrance slit with a spectrometer. The resulting streak image allows analysis of the temporal- and spectral domain. It can also be used as a two dimensional detection device, by widening the entrance slit and turning off the sweep voltage, which is ideal when aligning the setup [5], [6].
The Microchannel plate (MCP) is an important component when using the streak camera, because it achieves reliable signal amplification [6]. Primary electrons, entering the channel

will produce secondary electrons when hitting the channel's wall. This process is repeated several times, until an electron avalanche exits the tube on the end side. The cross section of one MCP channel is shown in figure 5. Note, however, that a whole MCP consists of several of such channels.

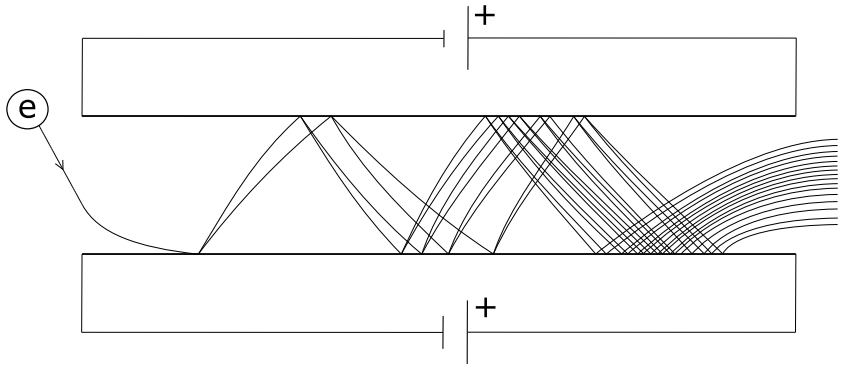

Figure 5: Schematic of the MCP. Reproduced from [6].

2.3 Laser Induced Fluorescence LIF

Rhodamine B, also called Rhodamine 610, is a fluorescent dye. It can be used for measuring temperature, because its quantum yield is highly dependent on temperature, making the intensity and the lifetime of its fluorescence strongly temperature dependent [10]. Additionally, it is relatively cheap and not particularly harmful in a health perspective [11].
There are many ways to excite an atom or molecule, meaning exciting one of its electrons from a lower to a higher energy level. This can be done by, for example, absorbing of a photon with energy $\hbar \cdot \omega_p$ corresponding to the energy difference of the two levels, $\Delta E = E_{final} - E_{initial}$. If this atom subsequently loses its additional energy spontaneously by the emission of photons, it is called fluorescence.
In LIF, the laser is tuned to resonance, ΔE, to selectively excite the atom or molecule, which can then lead to fluorescence emission. However, one has to take into account, that there are multiple processes by which the atom or molecule can lose its energy, which direct emission of photons is one of the least likely. More likely is the so-called quenching. This is a non-radiative, temperature dependent process, in which the specimen loses its energy via collisions [12]. A basic excitation and emission scheme in a LIF experiment is shown in figure 6.

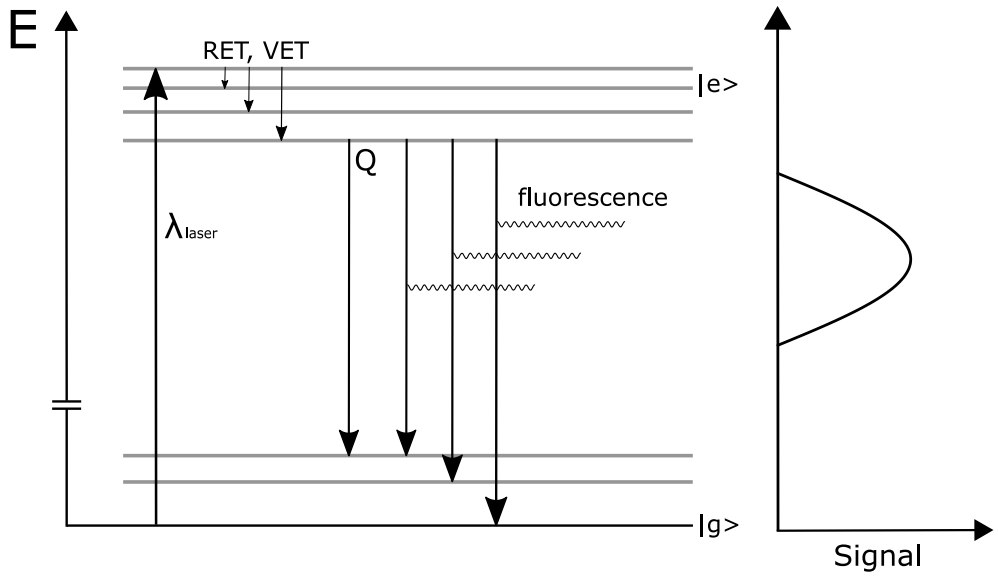

Figure 6: Basic excitation and emission scheme of a multilevel system. There are multiple ways to lose energy after excitation through, e.g. rotational/vibrational electronic transitions (RET, VET), quenching or fluorescence.

Furthermore, the recorded emission spectrum is red-shifted, also called stokes-shifted, which means wavelengths longer than the resonance wavelength are observed. This results from the fact that the de-excitation most likely occurs in a multi-part process. The atom or molecule first loses energy non-radiatively, e.g. through rotational/vibrational electronic transitions before de-exciting completely through quenching processes or fluorescence. There are always multiple electronic levels involved in the process, especially in complex molecules. The time it takes for the atom to get back into the initial state is called the fluorescent lifetime τ. In this work, only quenching and spontaneous emission will be treated in the LIF. In this model, the lifetime can be related to the respective coefficients $Q_{2,1}$, the quenching rate constant, and $A_{2,1}$, the Einstein coefficient for spontaneous emission, by

$$\tau = \frac{1}{A_{2,1} + Q_{2,1}}, \tag{5}$$

of which again the quenching factor $Q_{2,1}$ is the dominant one. [12], [13]
Here, the lifetime of the fluorescence can be related to the intensity decay via a mono exponential [10]

$$I(t) = I_0 \cdot \exp(-t/\tau), \tag{6}$$

where I_0 is the intensity instantaneously after excitation and t the elapsed time.

3 Periodic shadowing technique

Periodic shadowing is mainly inspired by lock-in amplification. Lock-in amplifiers were first build in the 1930s and have been used ever since to increase the signal-to-noise ratio in time dependent measurements. The idea of lock-in amplification is to extract one small frequency width and efficiently reject all other frequencies. It is particularly powerful in very noisy environments, where the signal of interest could vanish in the noise. [14]
Typically, the signal is centred around the origin in the Fourier domain which corresponds to the DC component. Noise, however, is typically also embedded at low frequencies, so the actual signal can be hard to isolate from other interference signals in either the spatial or Fourier domain. This is where lock-in amplification is useful. If the measurement signal is somehow superimposed with a periodic pattern, mathematical tools can help isolate the signal from the noise. In lock-in amplification, this is done in the time domain, by using for example an optical chopper. However, this can also be done in a similar way in measurements in a spatial domain, by using a grating, which is what is done in periodic shadowing [7]. By mounting the grating at the entrance slit of the spectrometer the signal is modulated, meaning a periodic pattern is superimposed onto the signal. The key of the methods is that parts of the signal that does not perfectly end up where it should, will lack this superimposed pattern. This part of the signal can be considered an interference and is a result of imperfections in the detector and the system that images the slit at the detector. The pattern can be easily identified in the Fourier domain as long as it is periodic. This is obvious, since any periodic function can be Fourier transformed into a finite sum of cosine and sine terms. The following mathematical derivation, which for simplicity is carried out for a sinusoidal pattern, can be done for any periodic pattern. [14] The starting point is the signal's intensity [7],

$$I(t,x) = A(t,x) \cdot \sin\left(f_g x + \phi(t,x)\right) + B(t,x), \tag{7}$$

with $A(t,x)$ being the function of the signal of interest, which is to be isolated, and $B(t,x)$ the noise term. The periodic pattern is a simple sine function with frequency determined by the grating spacing f_g and some phase factor ϕ. $I(t,x)$ now will be multiplied with a reference function, having the same frequency, as the superimposed pattern. Technically speaking, the spacing of the grating has to be known exactly for the method to work optimally. The product can be written as

$$I_{\sin}(t,x) = A(t,x) \cdot \sin\left(f_g x + \phi(x,t)\right) \sin f_g x + B(t,x) \sin f_g x, \tag{8}$$

and using the relation

$$\sin a \sin b = \frac{\cos\left(a-b\right)}{2} - \frac{\cos\left(a+b\right)}{2} \tag{9}$$

equation (8) can be simplified to

$$I_{\sin}(t,x) = A(t,x)\left(\frac{\cos(\phi)}{2} - \frac{\cos(2f_g x + \phi)}{2}\right) + B(t,x)\sin(f_g x). \tag{10}$$

Three different frequency terms are now well separated in the Fourier domain. One DC term, one with $f = 2f_g$ and one with $f = f_g$. The signal lies in the DC term and can be well

isolated from the noise by using a low-pass filter. The filter has a cutoff frequency f_{cutoff}, which is somewhere between the DC and the f_g frequencies.

$$\Phi = e^{(f/f_{cutoff})^{-6}} \tag{11}$$

Multiplying the filter function and the Fourier transform of the signal of interest will isolate the DC peak and will allow for a smooth transition, meaning there is an allowed Gaussian frequency distribution around the frequency of interest. This works, because the convolution of two functions in e.g. time or space domain, is the same as multiplying their Fourier transformations.
After the filter, equation (10) becomes

$$I_{\sin,f}(t,x) = \frac{A(t,x)}{2}\cos(\phi). \tag{12}$$

To avoid the phase term ϕ, equation (7) can be multiplied with $\cos(f_g x)$ instead of $\sin(f_g x)$. The phase term then cancels out when the squares of the two remaining functions after the filter are added together

$$\sqrt{I_{\cos,f}^2 + I_{\sin,f}^2} = \frac{A(t,x)}{2}\sqrt{\sin(\phi)^2 + \cos(\phi)^2}. \tag{13}$$

And thus the signal can be reconstructed using the two intensity profiles

$$A(t,x) = 2\sqrt{I_{\cos,f}^2 + I_{\sin,f}^2}. \tag{14}$$

The overall procedure for a one dimensional measurement is visualized in the following figures.

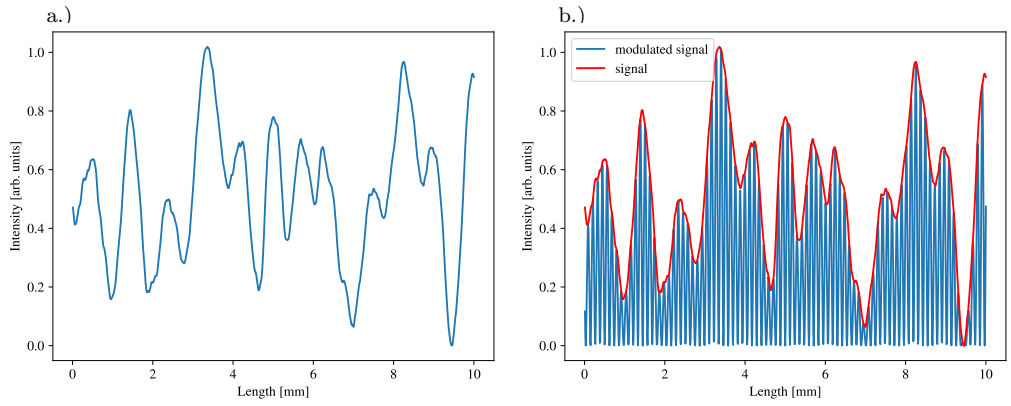

Figure 7: a.) A random computer generated signal to be processed and b.) the same signal modulated by lock-in methods.

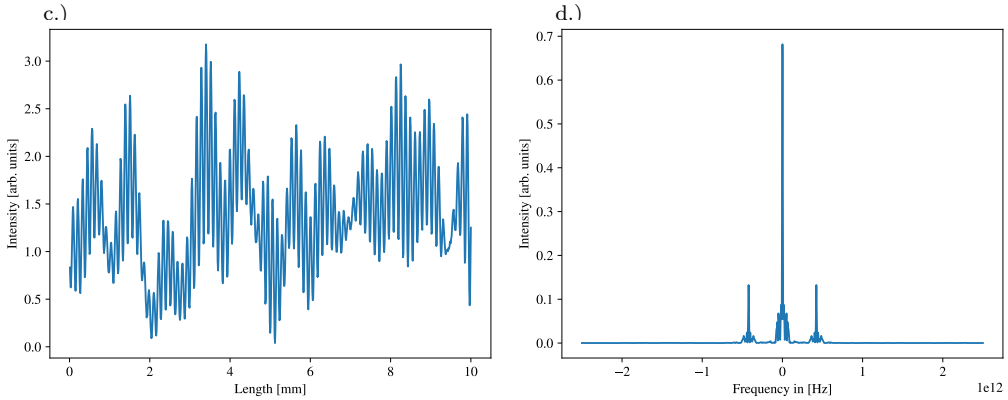

Figure 8: c.) Non-modulated background and noise added to b.). d.) Fourier transformation of c.).

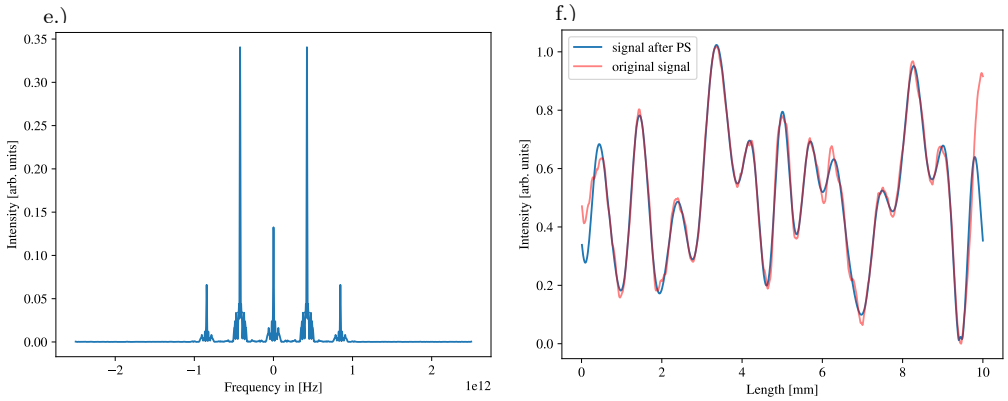

Figure 9: e.) Swapping of the position of the noise with the position of the signal, by multiplying with a reference signal. f.) The blue curve is the reconstructed signal from the DC peak in figure e.).

4 Experimental setup

A scheme of the experimental set-up is displayed in figure 10. The 532 nm mode-locked laser beam is directed through the RhB-water-solution, where the fluorescence is excited, and then blocked by the beam dump B1. F1 and F2 are filters and are used to prevent the light from damaging the streak camera. F1, a notch filter, filters out the laser beam, 532 nm, and F2, which is an ND-filter, reduces the overall intensity of the fluorescence light. In addition, a thermometer measures and displays the temperature of the dye/water solution. G1 is the mounted grating, in order to modulate the incoming signal before entering the detector. The two lenses in the double lens system, L1 and L2, have the same focal length of 200 mm. The distances D1, D2 and D3 are chosen to focus the fluorescence of RhB onto the entrance slit of the streak camera. A trigger signal is used to synchronize the pulsed laser and the streak camera.

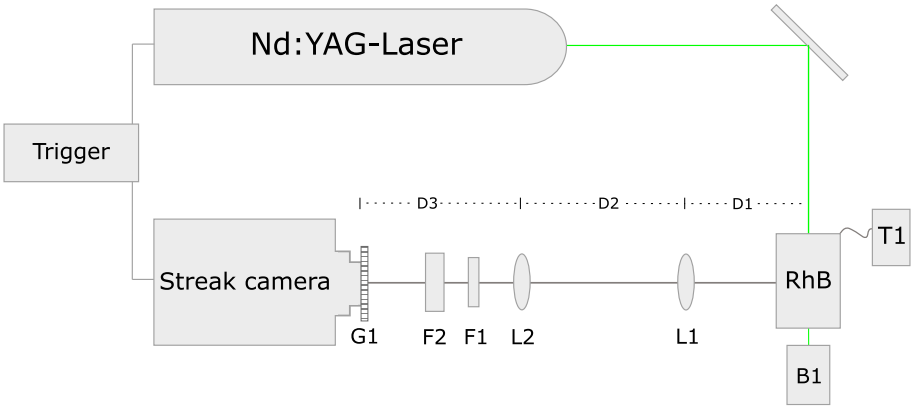

Figure 10: Schematic of the set up for the streak camera measurement.

The distances D1, D2 and D3 in figure 10 can be estimated according to the thin lens formula

$$\frac{1}{f1} = \frac{1}{D1} + \frac{1}{D2}, \frac{1}{f2} = \frac{1}{D2} + \frac{1}{D3}. \tag{15}$$

Rearranging gives

$$\rightarrow \frac{1}{f1} - \frac{1}{D1} = \frac{1}{f2} - \frac{1}{D3}, \tag{16}$$

$$\rightarrow \frac{1}{f1} + \frac{1}{f2} = \frac{1}{D1} + \frac{1}{D3}. \tag{17}$$

Since $f1$ and $f2$ are equal to 200 mm,

$$10\,\mathrm{m}^{-1} = \frac{1}{D1} + \frac{1}{D3}, \tag{18}$$

and D1 and D3 should be chosen to fulfil this condition. D2 can essentially be set to anything, depending on what the set up conditions allow.

5 Results and Discussion

The experimental work can essentially be divided into two sections. First, measurements were carried out, in order to find the optimal settings for further studies. The second part consisted of a more quantitative approach, evaluating the lifetime of the LIF signal for different temperatures ranging from 20.5°C to 73.3°C and comparing to previously published results from Mercadé-Prieto et al., in which Rhodamine B was excited using two-photon excitation and the corresponding fluorescence was detected with a hybrid NDD detector [10]. The relevant result of these previously reported results is found in the appendix (figure 26). For the first part, only single shot data are shown and examined, while in the second part multiple shots were averaged to smooth the plots for a more detailed analysis.

5.1 Parameter study

The most important parameter to be investigated here was the streak rate of the camera. The laser power output was kept at ≈ 33.3 mW and the grating had 5 line pairs per mm. Mainly, the rising edge of the temporally resolved fluorescence curve and its lifetime were examined, to determine the effect of periodic shadowing.
Figure 11 shows both the raw output data directly from the streak camera and processed image from measurements with the streak rate set to 1 ns/mm and 500 ps/mm. The gain of the MCP was set to the highest possible value (900 V). It should, however, be noted that this did not damage the camera, since the gain of the MCP only determines the amount of photo-electron multiplication. As long as the input signal onto the photocathode is kept low, no harm is done to the camera.
The first observation in figures 11 (a), (b) is that the modulation of the grating is visible. The y-axis is along the slit width, where the grating is placed, which makes the signal periodically modulated. A cross-section at discrete x-values shows the modulation, displayed in figure 13 for the 500 ps/mm streak rate. The x-axis in figures 11 is the time dimension of the camera, as is displayed in figure 4. The fluorescence decay can be shown by taking a cross section of a discrete y-value. Figure 11 (a) also shows that the 1 ns/mm streak rate does not make use of the entire time dimension which on one hand ensures that the entire signal is captured in but on the other hand the temporal resolution is not optimized. The 500 ps/mm streak rate, figure 11 (b), having a smaller time window, makes better use of the full time dimension and thus should in theory yield results with higher temporal resolution. Streak rates at 250 ps/mm rate or faster should be even more effective, however the time jitter of the different electrical components in the setup becomes relevant.
The jitter is represented by fluctuations of the position of the fluorescence on the time axis which in some cases will cause parts of the fluorescence signal to fall outside the sampling window. There exist multiple procedures to account for jitter. In this current work, a Matlab function was used to align the signals to compensate for the time jitter and make the curves overlap in time. The basic operation behind the function is the use of correlation which is mathematically described in equation 19. The basic idea is to first select one curve as reference that the other curves are matched to. The match between the reference (S_{ref}) and the curve (S_{new}) is found when the area of the product ($S_{ref} \cdot S_{new}$) reaches its maximum.

$$\left(S_{ref} \circledast S_{new}\right)(t) = \int S_{ref}(\tau) \cdot S_{new}(t+\tau) d\tau. \tag{19}$$

Another observation can be seen in the bottom plots of figure 11. The plots resemble the streak image after post processing the modulation. It is visible that the modulation works better on the bottom side of the plot, also seen on the raw data measurements. The upper half is more blurry compared to the bottom half. The reason for this is probably that the streak camera imaging electronics are not fully optimized in the upper part of the image. Because of this imperfection, only the lower part of the image, pixel interval 600 to 1000 pixels, was used in the signal analysis, as can be seen in figure 12.

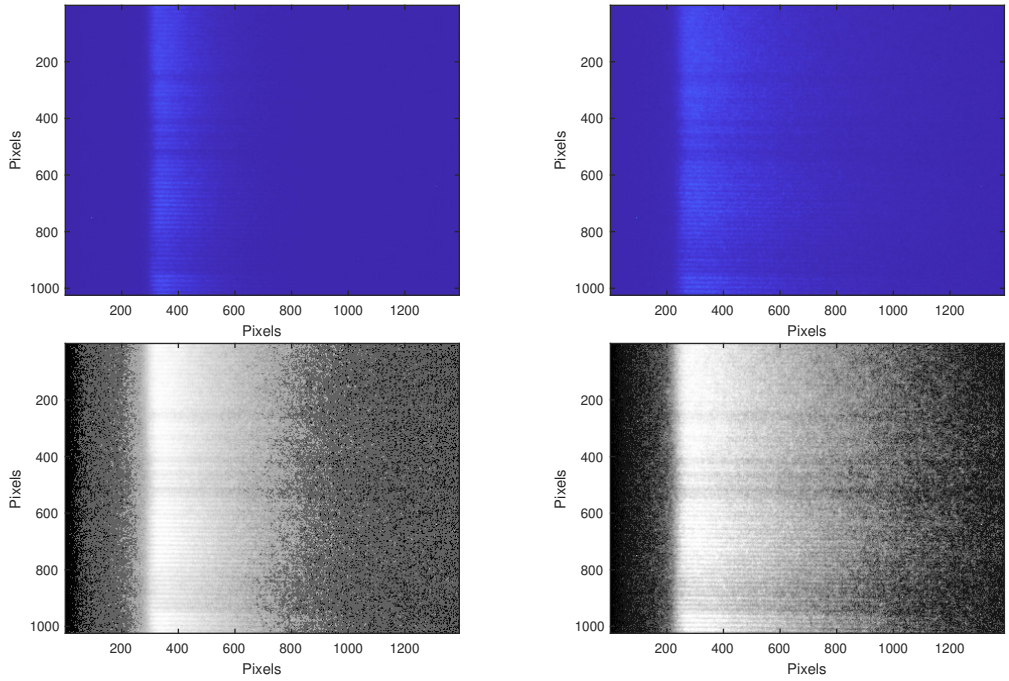

(a) Streak image using 1 ns/mm rate.

(b) Using 500 ps/mm rate.

(c) Streak image after periodic shadowing.

(d) Streak image after periodic shadowing.

Figure 11: The x-axis corresponds to the time and the y-axis to the spatial domain. Top: A single shot raw measurement acquired by the streak camera. Middle: Using high contrast on the image to make the modulation more visible (aesthetic reasons only). Bottom: The demodulated signal after post processing.

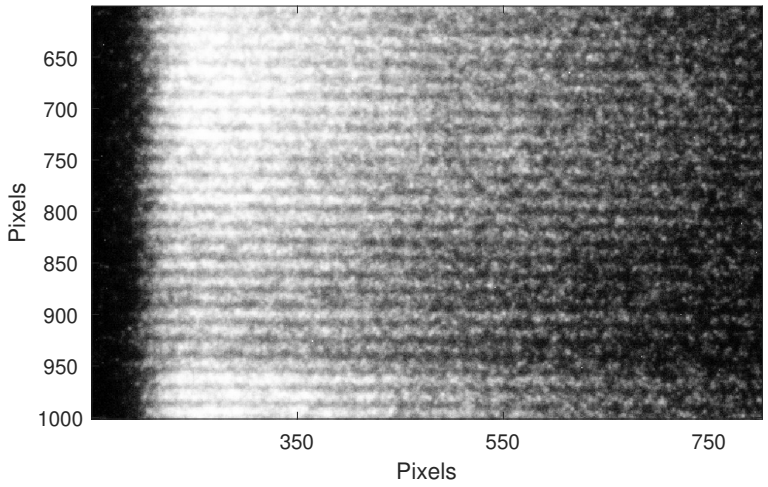

Figure 12: 500 ps/mm streak image of the used pixel interval (from figure 11 (b)).

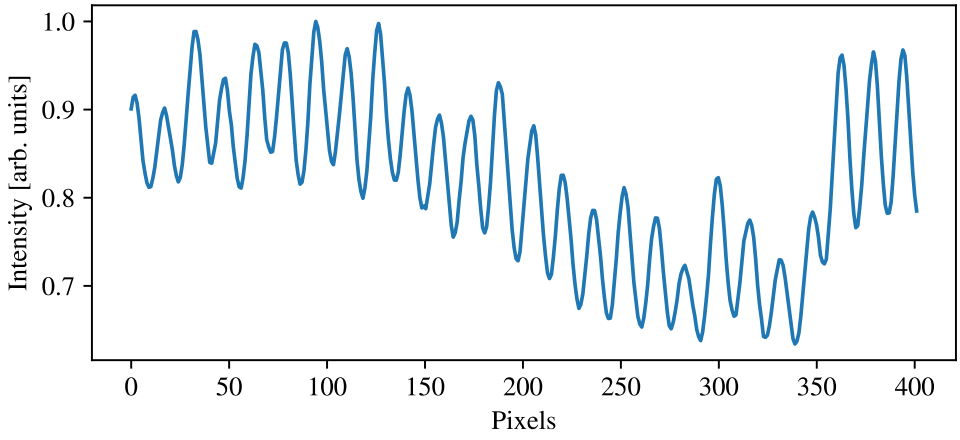

Figure 13: The inserted modulation for the 500 ps/mm streak rate in figure 12 (a) for the pixel interval from 600 to 1000 (normalized).

Figures 14 and 15 show the fluorescent decays, captured at a liquid temperature of 22°C, using different streak rates with and without the use of periodic shadowing. The conversion between pixels and time was achieved by an in-house made code for image analysis. Each curve is an average of 100 normalized signal shot curves. The reason for this is to reduce the noise and make shot-noise the dominating noise term. Still, the signal becomes noisier after applying the periodic shadowing scheme. This originates from the fact that at faster streak rates, the signal is more spread out, so the signal per pixel is lower, which in turn makes the signal-to-noise lower. An important anomaly visible in the plots can be seen in the beginning of the streak. There, the signal becomes negative. This also comes from the streak camera. The streak image has a overall noise offset which is subtracted in the processing part. The beginning of the streak image, however, has a lower offset and then rises for a short time until it reaches the right noise offset, this can be seen especially in the 25 ps/mm streak rate image in figure 15. It has not been solved what exactly causes this problem but it is most

likely related to the CCD in the streak camera.
A positive effect of periodic shadowing can be seen using all 3 streak rates in figure 14. The shape of the fluorescence rise becomes more sharp, as would be expected. With that, 100 ps/mm and lower streak rates, figure 15, have too small time windows to resolve a satisfactory amount of the decay and have significant jitter, so they were disregarded in further studies.

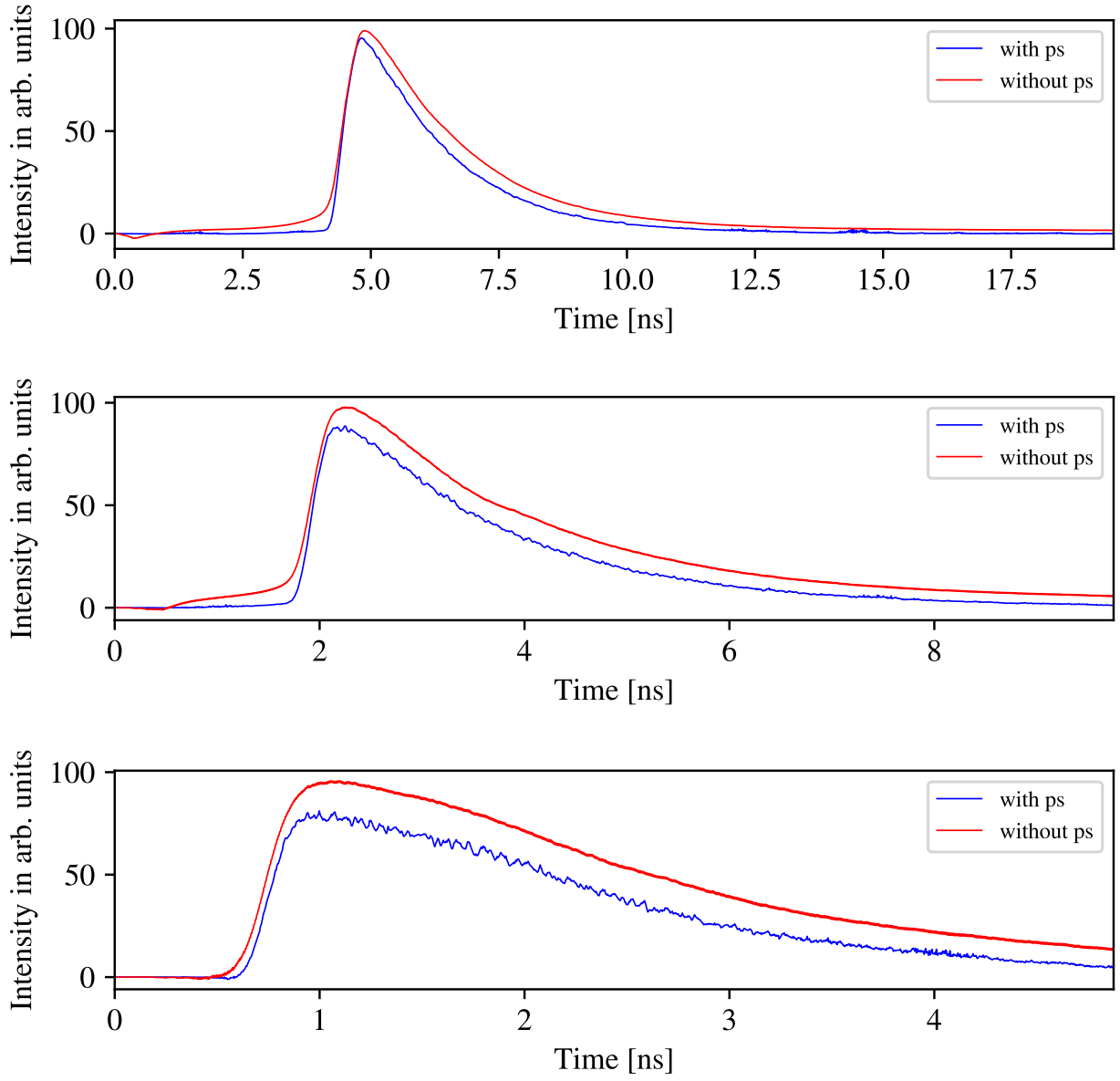

Figure 14: Fluorescent decay of RhB both with and without the use of periodic shadowing. Measurement to find optimal settings for further studies. 1 ns/mm (top), 500 ps/mm (middle) and 250 ps/mm (bottom) streak rates and laser power of 33.3 mW.

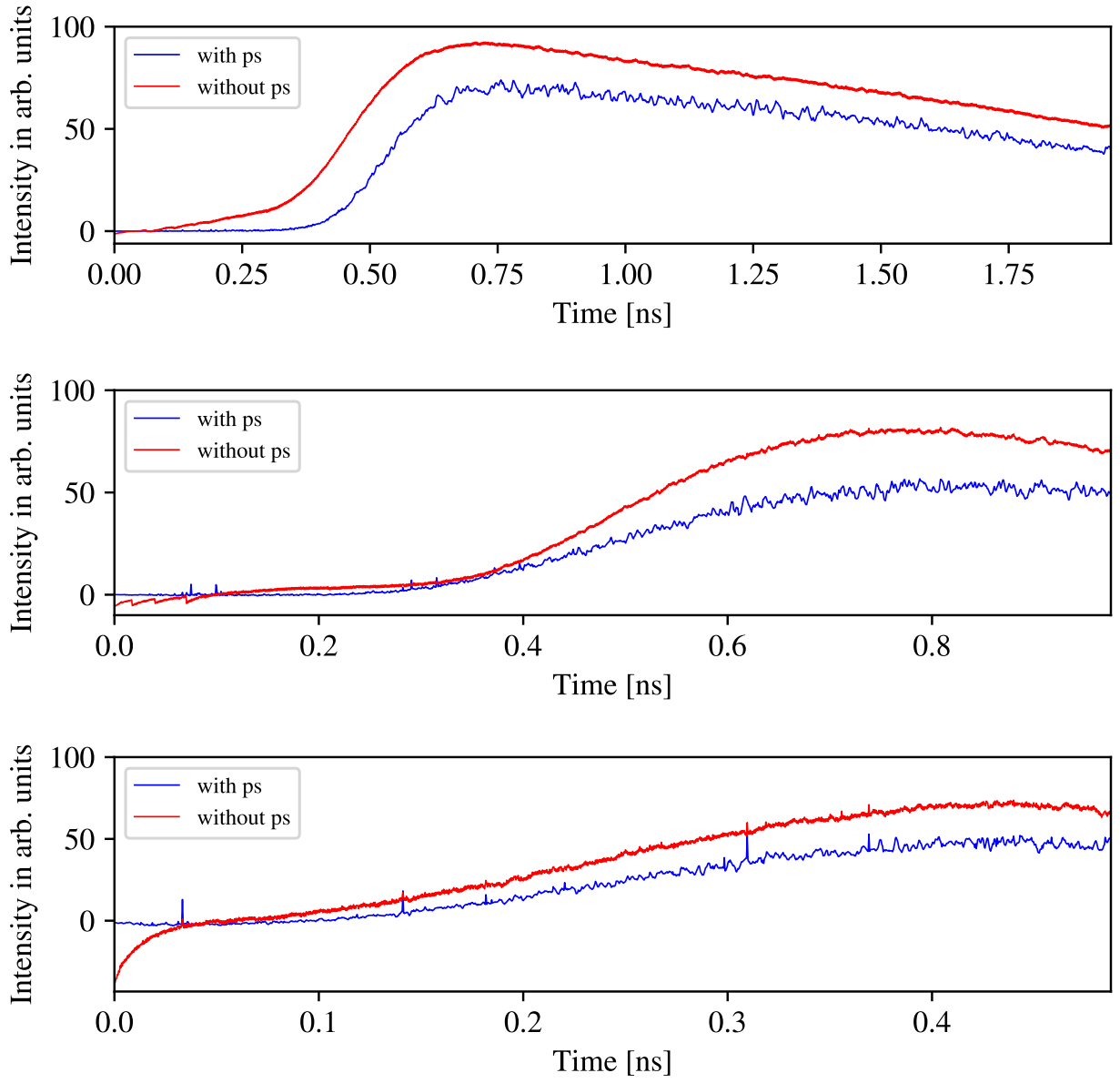

Figure 15: Fluorescent decay of RhB both with and without the use of periodic shadowing. Measurement to find optimal settings for further studies. 100 ps/mm (top), 50 ps/mm (middle) and 25 ps/mm (bottom) streak rates and laser power of 0.333 mW.

5.2 Lifetime study

The 500 ps/mm yielded the best result of 1.707 ns lifetime, compared to [10], in which it was found to be 1.7 ns at 21°C. The procedure of finding the lifetime starts with equation 6,

$$I(t) = I_0 \cdot \exp(-t/\tau),$$

taking the log of this expression

$$log(I(t)) = -t/\tau + log(I_0), \tag{20}$$

which means the slope m of the decay is directly relatable to the lifetime by

$$m = -1/\tau. \tag{21}$$

The next step was to find an interval, where log(I) best resembled a line equation and then make a first order fit to it using matlab.

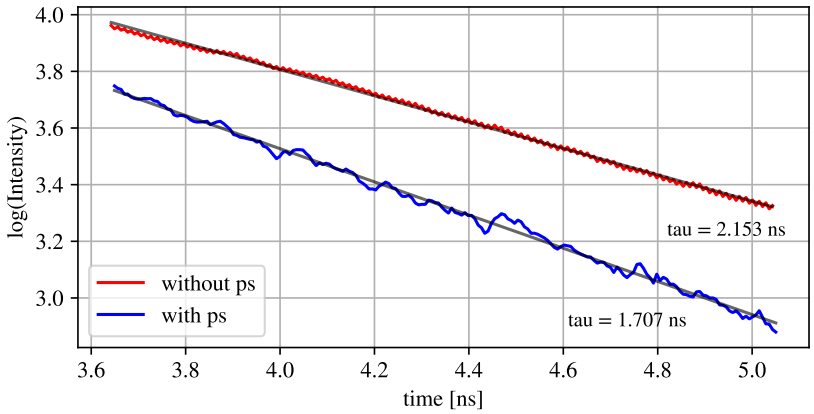

Figure 16: Lifetime calculation using linear fit on log(intensity) of 500 ps/mm streak rate measurements.

The second part of the experiment started with implementing a new CCD camera (Andor iStar CCD 334) into the streak camera system. The standard integrated CCD camera broke and had to be repaired so we introduced another CCD camera into the streak camera system. The new system changed slightly with respect to the old one, since the new chip had different dimensions, as displayed in figure 17. The streak rate 500 ps/mm was used to capture LIF decay curves in all measurements to determine the relationship between decay rates and temperature. As expected, the fluorescence is shorter for higher temperatures since the collision frequency increases with temperature in a liquid. One difference in this set up compared with the old one was that the spatial dimension did not cover the whole slit, which is clearly seen when figure 11 and figure 18 are compared. The demodulated spectrum is now zoomed in on the bright spot of figure 11. This is not a problem, since this is the part which was used in the analysis of the data captured with the initial setup. Also, the signal-to-noise ratio of the raw data is a lot better with the new camera. Furthermore, originating from a non optimal setup is that the data is slightly tilted. This is not straight forward to solve, because simply tilting the data back misaligns the pixels. In figure 19, the inserted modulations of the two systems are shown. Both modulations are normalized with respect to the measurement from the new camera. The figure, again, empathizes the difference in quality of the two used CCD cameras and that the new CCD, having a better resolution, inserts the modulation more accurately.

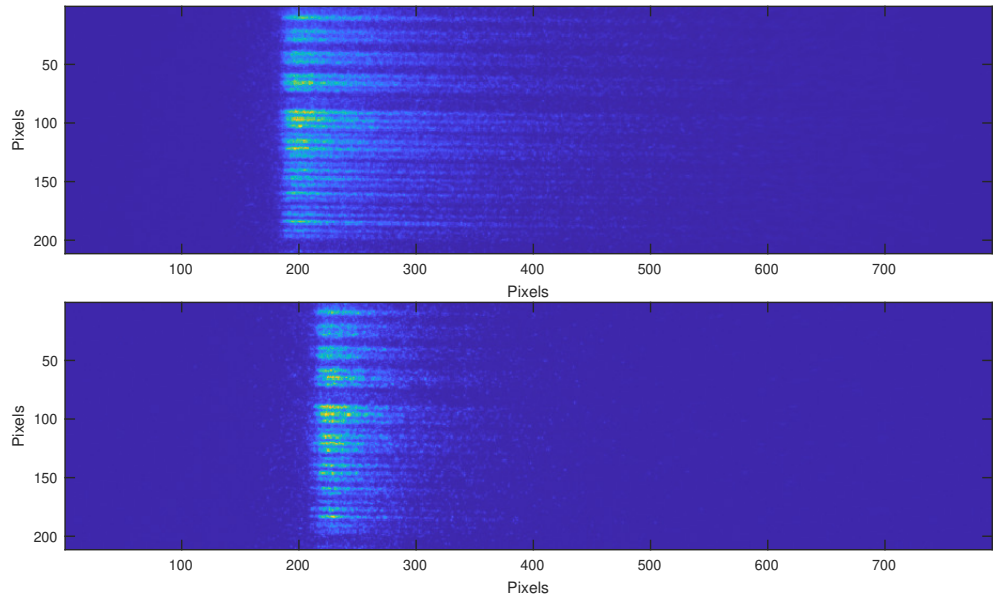

Figure 17: New CCD camera using 500 ps/mm streak rate, top: temperature of the dye 30°C, bottom: 73°C; notice the different dimensions of the camera in comparison to the old, figure 11.

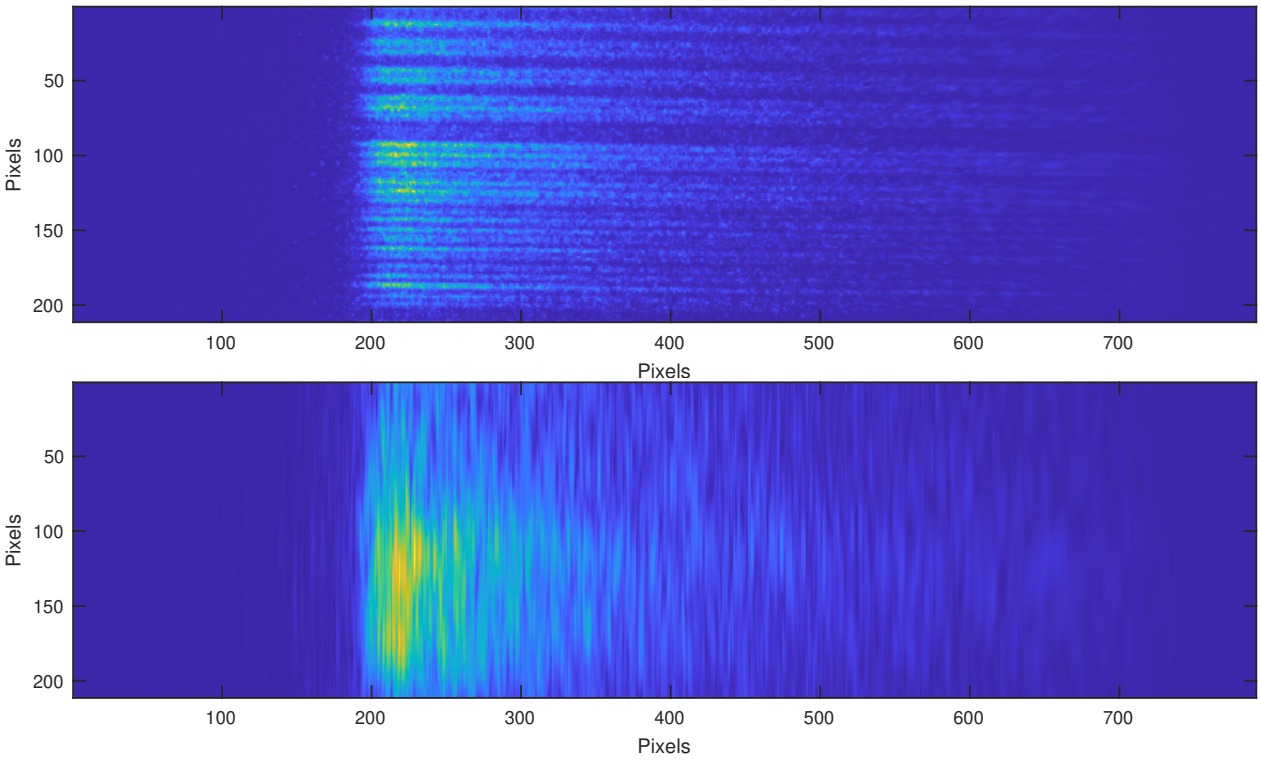

Figure 18: New camera results: 250 ps/mm, shows the effect periodic shadowing has on the demodulation.

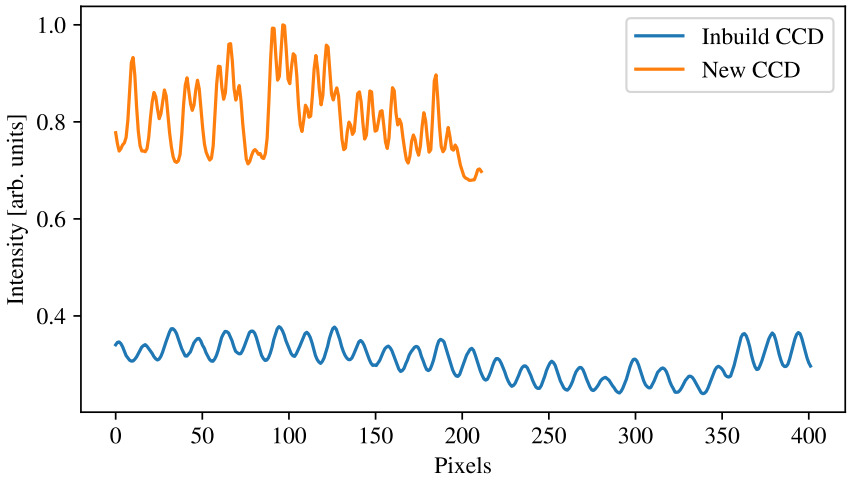

Figure 19: Modulations inserted using 500 ps/mm streak rate, shown for both the in-build CCD and the newly introduced CCD (both normalized onto the new CCD modulation).

A calibration of the system was necessary in order to determine the relation between pixels and time. Such measurements could be rather tedious to arrange and execute and could therefore not be fit into the time schedule. Instead, another approach was carried out where data sets, acquired with the streak rate of 500 ps/mm, were compared between the two setups.
The calibration was done by evaluating the lifetime from two near identical measurements in both setups. The time axis was then corrected for the new setup so that both measurements yielded the same lifetime. The calibration is shown here.

$$log(I_{oldcam}) = -C_1 \cdot t + b_1 \tag{22}$$
$$log(I_{newcam}) = -C_2 \cdot t + b_2, \tag{23}$$

$$C_1 = C_2 \cdot \frac{C_1}{C_2}, \tag{24}$$

Having this relation, the lifetime can now be calibrated for all measurements of the new camera using the old pixel-to-time relationship.

$$\frac{1}{\tau_{calibrated}} = \frac{1}{\tau_{newcam}} \cdot C_1/C_2, \tag{25}$$

$$\rightarrow \tau_{calibrated} = \tau_{newcam} \cdot C_2/C_1. \tag{26}$$

With a different set up, there is the possibility of relating back to the previous defects which were found in the data that was acquired with the first setup. Figure 20 shows the fluorescent decays of 1 ns/mm, 500 ps/mm and 250 ps/mm streak rates with the same temperature as the measurements of the old system. Since the readout time of the new camera was significantly longer, only 11 plots were superimposed in this measurement to ensure that the temperature

was the same in all data acquisitions. Nonetheless, there are visible differences between these results and the results that are shown in figure 14 where the difference between with and without periodic shadowing is smaller. It can be safely assumed that the new camera has better imaging characteristics than the original one. Although the number of pixels in each dimension of the new CCD is lower, the new camera has a significantly better quantum efficiency, meaning it is more sensitive to light. It also has its own post-processing noise cancelling routine, which in turn makes the readout time a lot more longer than the readout time of the old camera. To compare, in the old setup the pulsed laser was running at 5 Hz, while in the new setup it was running with 0.2 Hz. In general, it can be said that the quality of the new camera and especially the chip is a lot better.

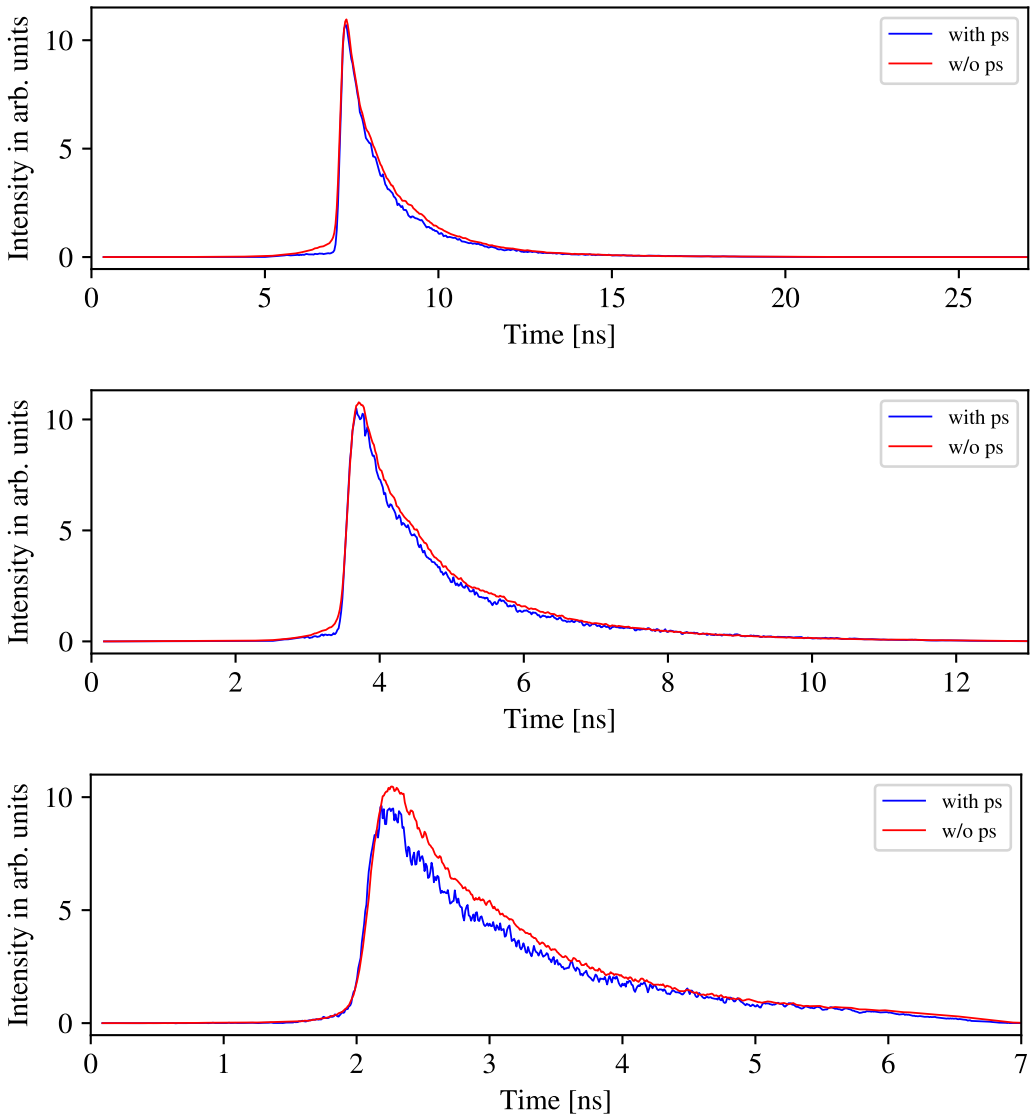

Figure 20: Fluorescent decay of RhB both with and without the use of periodic shadowing. Data taken with the new camera set up. 1 ns/mm (top), 500 ps/mm (middle) and 250 ps/mm (bottom) streak rates and laser power of 50 mW.

Below, the three measurements are shown for 1 ns/mm, 500 ps/mm and 250 ps/mm streak rates.

Temp [°C]	τ_{conv} [ns]	τ_{ps} [ns]
20.5	2.37	2.07
27.0	2.27	2.01
42.75	1.83	1.58
58.6	1.41	1.18
62.95	1.33	1.09
70.5	1.29	1.09

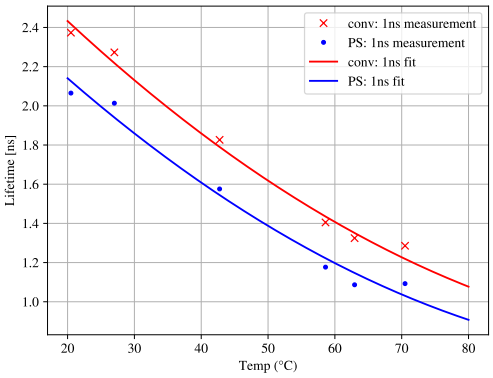

Figure 21: 1 ns/mm: Temperature and lifetime measurements and the corresponding second degree polynomial fits.

Temp [°C]	τ_{conv} [ns]	τ_{ps} [ns]
20.5	1.82	1.72
30.15	1.71	1.66
45.85	1.36	1.33
59.05	1.16	1.05
63.35	1.00	0.931
72.2	0.956	0.919

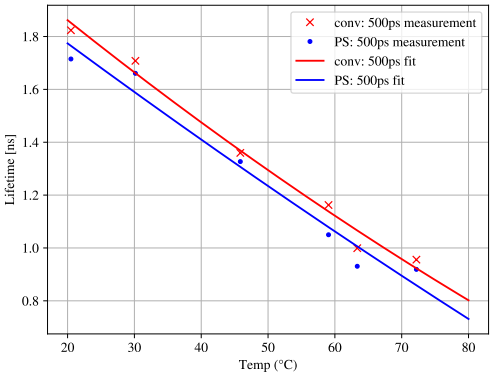

Figure 22: 500 ps/mm: Temperature and lifetime measurements and the corresponding second degree polynomial fits.

Temp [°C]	τ_{conv} [ns]	τ_{ps} [ns]
20.5	1.88	1.81
33.05	1.52	1.45
47.5	1.16	1.10
59.25	0.866	0.791
64.6	0.817	0.775
73.55	0.691	0.688

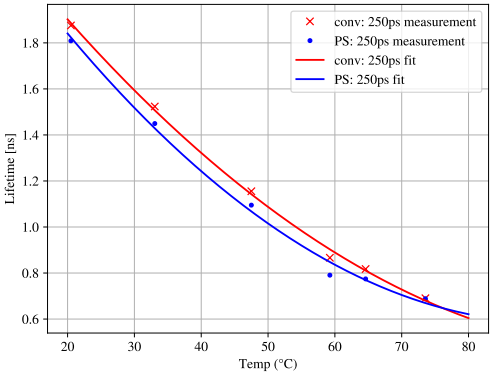

Figure 23: 250 ps/mm: Temperature and lifetime measurements and the corresponding second degree polynomial fits.

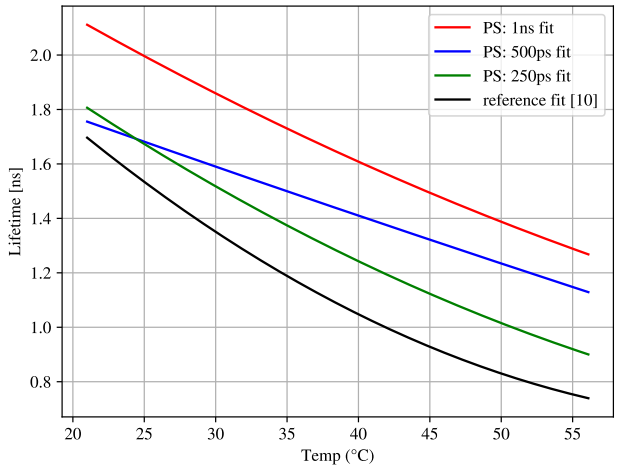

Figure 24: The curves of the three streak rates after periodic shadowing and a corresponding curve as mentioned determined in [10].

Comparing to the evaluated curve by [10], the 250 ps/mm with periodic shadowing (green curve in figure 24) yields the best result. The corresponding second-degree fit,

$$\tau = aT^2 + bT + c, \tag{27}$$

gives parameters $a = 2.36$, $b = -4.43 \cdot 10^{-2}$ and $c = 2.40 \cdot 10^{-4}$. At 21°C our model gives 1.806 ns and at 56°C yielding 0.9019 ns. Comparing to the model by [10]: 1.7 ns at 21°C and 0.74 ns at 56°C. This means our model both has an offset and also is not steep enough, meaning it drops too slowly with increased temperature. Apart from that, the effect of periodic shadowing is clearly visible. Every calculated value of the fluorescence lifetime corresponds better to previously published data after making use of the modulation and the periodic shadowing processing, visible in figures 21, 22 and 23.

Although the streak camera can be used to examine lifetimes in detail, one shortcoming exists. The streak camera is a two dimensional device, able to resolve not only time varying but also one dimensional spatially varying processes. When determining the lifetime of Rhodamine B, for example, there is no use of a spatial dimension in this current investigation. The spatial dimension was only used during these experiments to insert the modulation.
Given this and that periodic shadowing can be implemented in a measurement, the next step is, to measure a process that extends both in a spatial and time domain. One such experiment is seen in figure 25. The laser is focused onto a point placing a lens in its beam path. At the focus point, the energy density is so high that a plasma is created. The radiating plasma can be seen as the very bright object in figure 25. Somehow, the creation of the plasma creates a second focus point spatially apart which can be seen in the image as the less bright object.

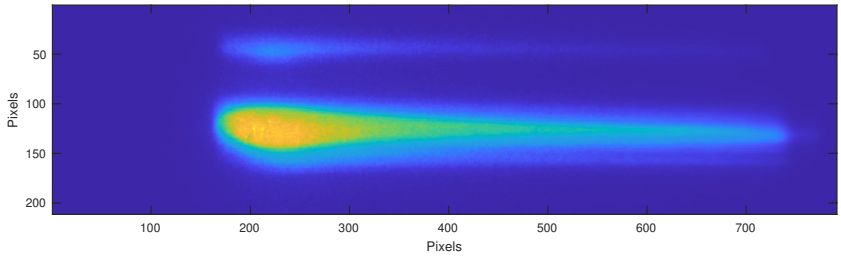

Figure 25: Streak camera image of a plasma creation by focusing a laser down to a point.

6 Conclusion

This work is the first of its kind where periodic shadowing is used with a streak camera and it should be highlighted that this investigation showed that periodic shadowing is capable of improving contrast when it is applied to a streak camera. Especially the measurements involving the first CCD camera show great improvements with periodic shadowing. It can thus be concluded that a large amount of interfering signal seems to stem from the CCD camera itself. However, a significant improvement in the shape of the fluorescence, supported by a more accurate lifetime yield, is observed in measurements of both cameras. The maximum improvement in lifetime was approximately 20 %, achieved with the 1 ns/mm streak rate. Another powerful aspect of periodic shadowing is the implementation into the experiment. Practically, it adds low additional effort. The main part involves finding a suitable grating, by looking at the available resolution. Furthermore, it normally will not add much expenses, since a variety of gratings are available in most laboratories.
Looking at Rhodamine B, the lifetime and temperature dependency was observed and additionally this correlation seem to be stable, which makes RhB a good candidate for mapping the temperature gradients in microfluids.
It is clear that this first test of applying periodic shadowing in combination with a streak camera shows promising potential and should be further investigated.

7 Appendix

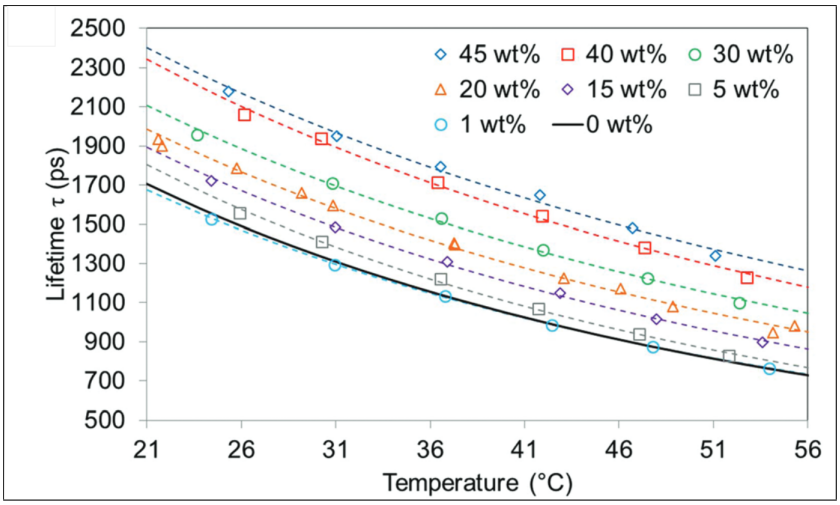

Figure 26: Lifetime plot of the RhB paper, only the black solid line is of interest since only this measurement data is captured from a pure water/dye solution. [10]

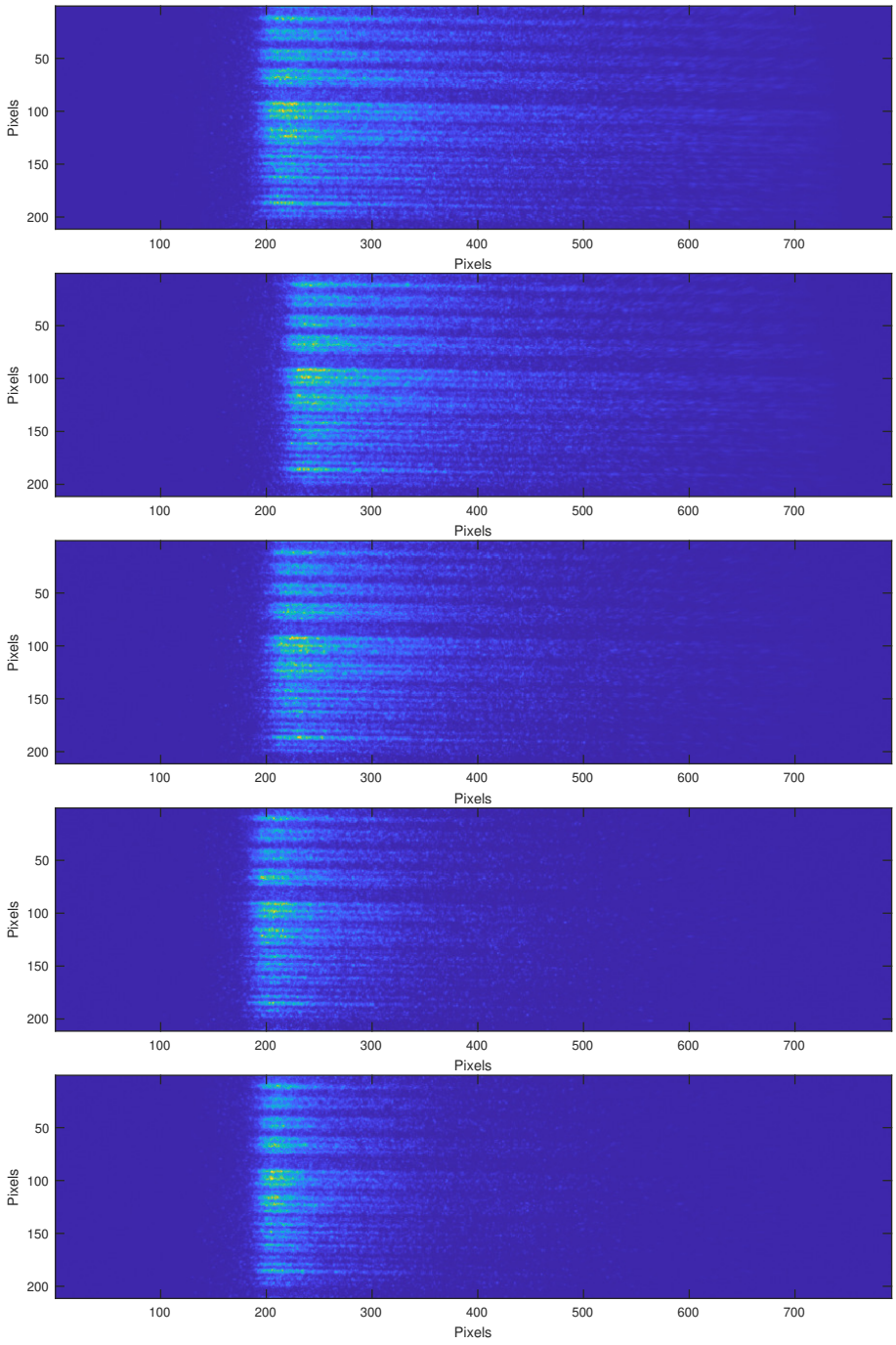

Figure 27: Temperature change of the streak images using 250 ps/mm streak rate.

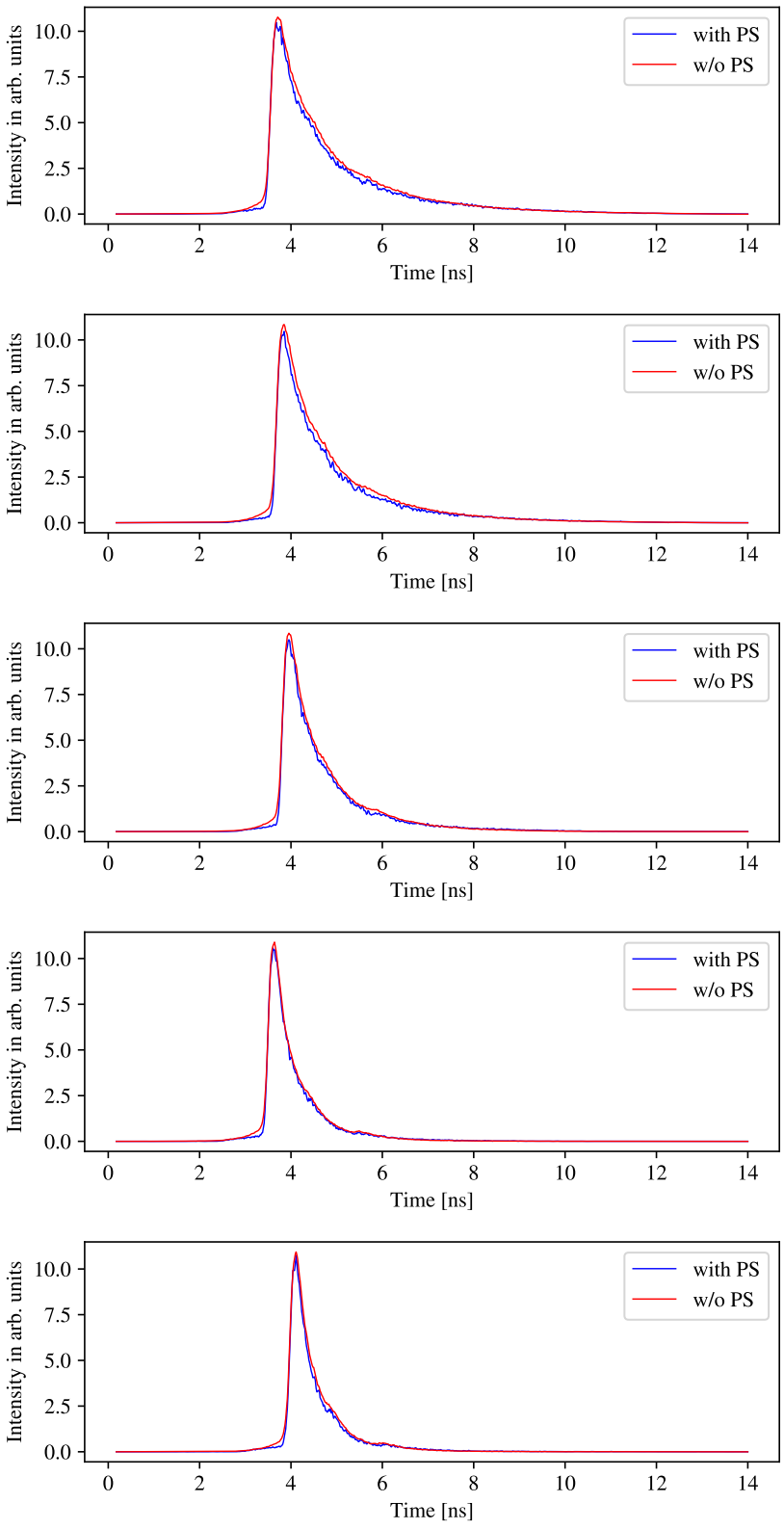

Figure 28: Temperature change of the fluorescence using 500 ps/mm streak rate (range from 21°C (top) to 72°C (bottom)).

References

[1] J. Michael Hollas. *Modern Spectroscopy 4th Edition*. John Wiley & Sons, 2004. ISBN: 0470844167.

[2] Per Augustsson. "On microchannel acoustophoresis: Experimental considerations and life scienc eapplications". PhD thesis. Lund University, 2011.

[3] Mahdi Rezayati Charan, Per Augustsson. "Charting cell properties through their acoustophoretic migration in a gradient of density and compressibility". Acoustofluidics Conference. 2020.

[4] Wei Qiu, Per Augustsson et al. "Thermal-gradient-induced fast convection in acoustofluidic devices". Acoustofluidics Conference. 2020.

[5] Andreas Ehn. "Towards Quantitative Diagnostic Using Short-Pulse Laser Techniques". PhD thesis. Lund University, 2012.

[6] Hamamatsu. *Streak camera*. URL: `https://www.hamamatsu.com/eu/en/product/photometry-systems/streak-camera/index.html`. (accessed: 14.12.2020).

[7] Elias Kristensson, Andreas Ehn et al. "Stray light supression in spectroscopy using periodic shadowing". In: *Optics Express* (2014). DOI: `10.1364/OE.22.007711`.

[8] Rüdiger Paschotta. *Mode Locking*. URL: `https://www.rp-photonics.com/mode_locking.html`. (accessed: 14.12.2020).

[9] Wolfgang Demtröder. *Demtröder Experimentalphysik 3, 5th Edition*. Springer Spectrum, 2016. ISBN: 978-3-662-49093-8.

[10] Ruben Mercadé-Prieto et al. "Fluorescence lifetime of Rhodamine B in aqueous solutions of polysaccharides and proteins as a function of viscosity and temperature". In: *Photochemical & Photobiological Sciences* (2017). DOI: `10.1039/C7PP00330G`.

[11] Sigma-Aldrich. *Safety Data Sheet*. URL: `https://www.sigmaaldrich.com/MSDS/MSDS/DisplayMSDSPage.do?country=SE&language=de&productNumber=r6626&brand=SIGMA&PageToGoToURL=`. (accessed: 14.12.2020).

[12] A.C. Eckbreth. *Laser diagnostics for combustion temperature and species 2nd edition*. Gordon and Breach, 1996. ISBN: 90-5699-532-4.

[13] Andreas Lantz. "Application of Laser Techniques in Combustion Enviroments of Relevance for Gas Turbine Studies". PhD thesis. Lund University, 2012.

[14] Zurich Instruments. *Principles of Lock-in Detection*. URL: `https://www.zhinst.com/europe/en/resources/principles-of-lock-in-detection`. (accessed: 14.12.2020).